IEEE Photonics Journal
An IEEE Photonics Society Publication

Open Access

Large-Scale Integrated Multi-Lines Optical Phased Array Chip

Volume 12, Number 4, August 2020

Lan-Xuan Zhang
Ying-Zhi Li
Min Tao
Yu-Bing Wang
Yu Hou
Bo-Song Chen
Yu-Xuan Li
Li Qin
Feng-Li Gao
Xian-Shu Luo
Guo-Qiang Lo
Jun-Feng Song

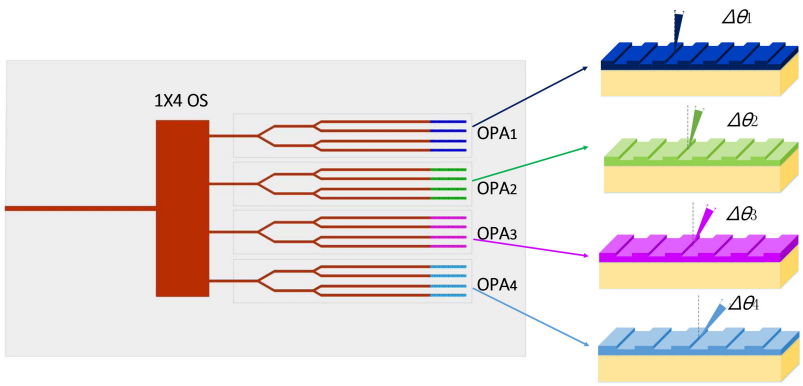

DOI: 10.1109/JPHOT.2020.3001005

Large-Scale Integrated Multi-Lines Optical Phased Array Chip

Lan-Xuan Zhang,[1] Ying-Zhi Li,[1] Min Tao,[1] Yu-Bing Wang,[2,3] Yu Hou,[1] Bo-Song Chen,[1] Yu-Xuan Li,[1] Li Qin,[2,3] Feng-Li Gao,[2] Xian-Shu Luo,[4] Guo-Qiang Lo,[4] and Jun-Feng Song [1,3]

[1]State Key Laboratory on Integrated Optoelectronics, College of Electronic Science and Engineering, Jilin University, Changchun 130012, China
[2]State Key Laboratory of Luminescence and Application, Changchun Institute of Optics, Fine Mechanics and Physics, Chinese Academy of Sciences, Changchun 130012, China
[3]Peng Cheng Laboratory, Shenzhen 518000, China
[4]Advance Micro Foundry Pte. Ltd., Singapore Science Park II 117685, Singapore

DOI:10.1109/JPHOT.2020.3001005

Manuscript received February 25, 2020; revised May 13, 2020; accepted June 4, 2020. Date of publication June 9, 2020; date of current version June 30, 2020. This work is supported by the National Key R&D Program of China under Grant No. 2016YFE0200700, and the National Natural Science Foundation of China under Grants No. 61627820 and No. 61934003. Corresponding author: Jun-Feng Song (e-mail: songjf@jlu.edu.cn).

Abstract: We design and integrate four optical phased arrays (OPAs) in a single chip. Each OPA possesses different output grating period. Furthermore, we use optical switches to select one or more OPAs for beam scanning. We demonstrate the longitudinal scanning by tuning the laser wavelength. The experimental results show that the scanning range of the four-lines chip reaches 28.54° when the wavelength ranges from 1520 nm to 1570 nm, and the eight-lines one reaches 19.04° with wavelength range of 1520 nm-1540 nm. We greatly improve the wavelength tuning efficiency for longitudinal scanning.

Index Terms: longitudinal scanning, tuning efficiency.

1. Introduction

Light Detection and Ranging (LiDAR) has the advantages such as large angle, large range, and high speed resolution [1]. It has a broad applications in airborne, driver-less vehicle borne radar and autonomous robot. The traditional mechanical LiDAR module consists of a set of optical components and electronic components. Due to its large size, potentially low reliability and particularly prohibitively high cost, it could be difficult to achieve with mass production [2]. In recent years, with the development of photonic integrated circuits, the integration of thousands of photonic elements on a single chip becomes possible [3].

Optical Phased Array (OPA) is a beam forming and steering technology [4]–[15]. Each waveguide in the OPA is equivalent to a slit in multi-slit interference apparatus, light from the waveguide will interfere in the air. As a result, the power of the light is enhanced in certain direction and weakened in other directions by the interference, the scanning beam forms in this case.

Horizontal wide field of view has been demonstrated in the past. Aperiodic arrays designed by ordered non-uniform spacing, global search algorithms and pattern search algorithms have achieved large-scale scanning range [16], [17]. Another creative solution is the anti-crosstalk design with unequal width waveguide and true half-wavelength emitter pitch [18]. Scanning in the

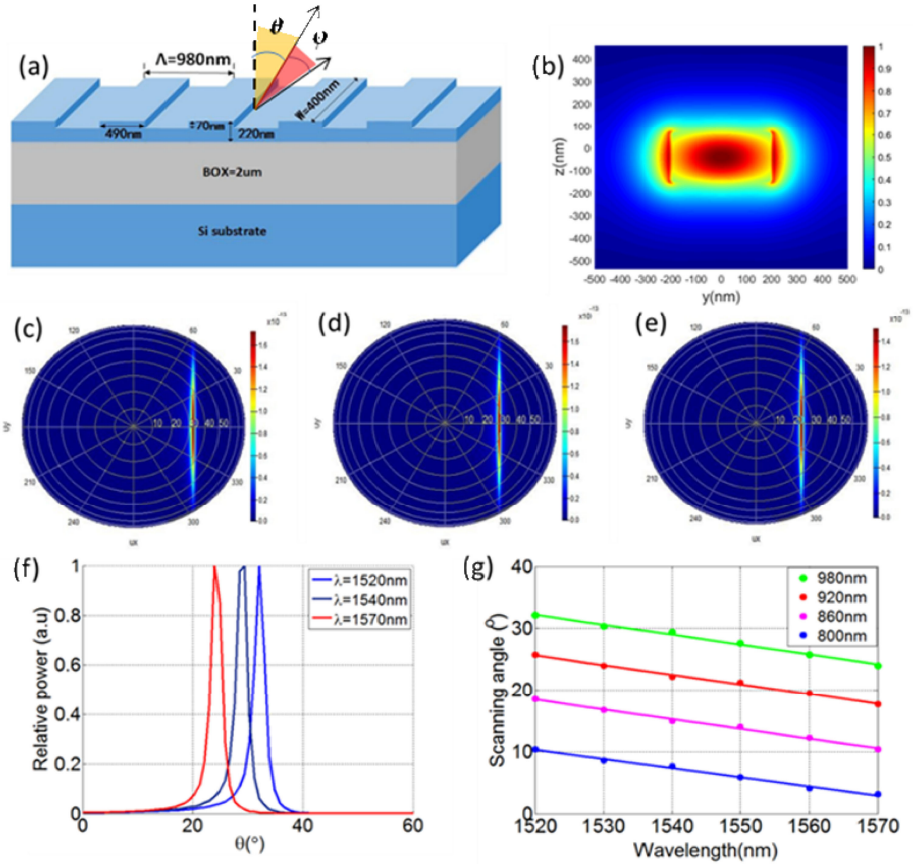

Fig. 1. Simulation results of Lumerical FDTD (a) Schematic diagram of grating. (b) Light with TE mode. (c), (d), and (e) Far-field distributions when the light with wavelengths of 1520 nm, 1540 nm, and 1570 nm respectively in grating whose period is 980 nm. (f) Normalization of intensity at $\varphi = 0$ in Fig. 1(c), (d), and (e). (g) For waveguide gratings with period of 980 nm, 920 nm, 860 nm and 800 nm, when the incident light changes from 1520 nm to 1570 nm, the beam steering is simulated.

longitudinal direction can be realized by changing the wavelength of the laser when the grating is fabricated on optical waveguide [19]–[24]. Acoleyen *et al.* tuned the optical wavelength from 1500 nm to 1600 nm to realize beam steering with 14.1°, with the tuning efficiency of 0.14°/nm [25], Hutchison *et al.* adjusted the wavelength from 1260 nm to 1360 nm to achieve the angle deflection of 17° with an efficiency of 0.17°/nm [26]. To the best of our knowledge, the highest tuning efficiency reported is 0.3°/nm [27]. It seems that due to the relatively weak grating angle dispersion capability, the tuning efficiency is rather low when tuning the wavelength for beam scanning.

In this work, we integrated four OPAs on a single chip in order to overcome the limitation of small longitudinal beam emission scanning area obtained in a limited wavelength range. Each OPA can point to different direction. The four OPAs can be selected by thermo-optic switch. Collectively, a large beam emission area can be obtained because the scanning range of the entire chip is the sum of the scanning ranges of the four OPAs. Two different devices have been designed and implemented, with 28.54° (0.57°/nm) and 19.04° (0.95°/nm) beam steering range in the longitudinal direction.

2. Design of Waveguide Grating Array

we use Lumerical Finite Difference Time Domain (FDTD) tools to design the antenna structure [28]. Fig. 1(a) shows the schematic cross-sectional view of a waveguide grating. The waveguide

TABLE 1
Parameters for the FDTD

Source mode	Mesh step setting (nm)			Boundary conditions		Simulation temperature(K)	Simulation time (fs)
	x mesh	y mesh	z mesh	type	layers		
Fundamental TE mode	22	22	22	PML	8	300	2000

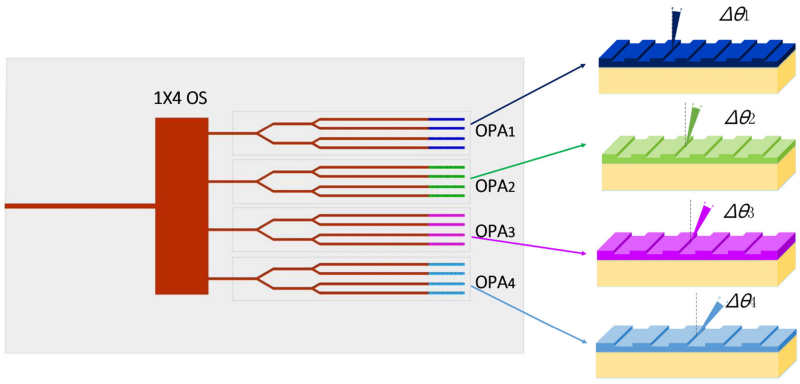

Fig. 2. Schematic diagram of the four-lines optical phased array chip. The grating periods of the four OPAs are different, and the scanned ranges are different.

is designed on the Silicon-On-Insulator (SOI) structure with top silicon thickness is 220 nm, and BOX thickness of 2 μm. The waveguide width is 400 nm. At the end of the waveguide, a grating is etched. The etching depth is 70 nm. We first simulated the performance of a single OPA in wavelength tuning. The parameters for the FDTD is shown in Table 1. The period of the grating is 980 nm with a fill factor of 50%. Assuming incident light with different wavelength is transverse-electrically (TE) polarized mode as shown in Fig. 1(b). Fig. 1(c)–(e) are respectively the far-field distributions with the wavelength of 1520 nm, 1540 nm and 1570 nm. Fig. 1(f) shows the extracted and normalized far-field distributions when the transverse angle is zero, i.e. $\varphi = 0°$. It can be seen that the beam points to 32.11°, 29.40° and 23.97° respectively in the θ direction. The single OPA can only scan 8.41° in θ direction when tuning 50 nm wavelength. We have also simulated the far-field of waveguide gratings with periods of 920 nm, 860 nm and 800 nm. When the modulation wavelength is increased from 1520 nm to 1570 nm, the radiation angle is shown in Fig. 1(g). It can be concluded that for grating antennas with fixed period, as the increase of incident wavelength, the radiation angle becomes smaller. Whereas for the same incident wavelength, the scanning angle with large grating period can be larger. The output beam angles of four gratings are 3.17° to 10.40°, 10.40° to 18.54°, 17.64° to 25.78° and 23.97° to 32.11° respectively for periods of 800 nm, 860 nm, 920 nm and 980 nm. The simulation results show that if we integrate the four periodic antennas, the range of out-coupling angle can reach 28.94°.

Based on such simulation, we integrate four OPAs with the above mentioned periods on a single chip. The schematic of the integrated photonic circuits is shown in Fig. 2. After the light enters the chip, it first passes through the 1 $\times$ 4 optical switch and gets into four different OPAs, each of which is composed of 16 optical waveguides. Each OPA has a different longitudinal pointing range ($\Delta\theta$) when the wavelength is tuned. Different colors in Fig. 2 represent different beam scanning ranges. The steering range of the entire chip is the splicing of scanning ranges of the four OPAs.

3. Fabrication and Experimentation

We fabricate the integrated photonics circuits using standard CMOS compatible Silicon Photonics Platform Process [29] in AMF, Singapore. Fig. 3 shows the optical microscope image of the chip.

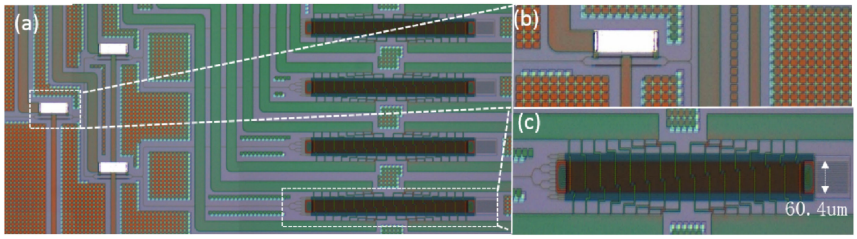

Fig. 3. (a) Optical microscope picture of four-lines optical phased array chip. (b) Single optical switch (c) Single OPA.

The three thermo-optical switches on the left of the chip compose a small 1 $\times$ 4 thermo-optical switch array with Mach-Zehnder interferometer (MZI) structure. The silicon waveguide width in the thermo-optical switch is 500 nm. The three optical switches can arbitrarily distribute the incident light among four OPAs. In each OPA, light is divided into 16 waveguides by multimode interference (MMI) beam splitters. The distance between waveguides is 4 μm. TiN is used as thermal heater, which is 1.5 μm away from silicon waveguides. The length of TiN on 16 waveguides presents linear gradient. Thus the applied phase on waveguide array also presents gradient. The chip footprint is about 2.2 mm $\times$ 3.5 mm.

3.1 Four-lines Optical Phased Array Beam Scanning

The experimental characterization system is shown in Fig. 4(a), and Fig. 4(b) shows its schematic. As the scanning beam is emitted from the upper end of the chip, a 45° reflector is placed directly above the chip to reflect the emitted beam to the receiving screen. The distance between the screen and the chip is 9 cm. The infrared camera converts the far-field pattern on the screen into a gray-scale signal and presents it on the display. The multi-channel power module is connected to the PCB in order to supply electrical signals to the thermo-optical switch. We use optical switch to select different OPA and tune the input light wavelength of each one.

The waveguide loss is 1.6 dB/cm, fiber to waveguide coupling loss is 2.5 dB/facet, and 1-by-2 MMI is 0.15 dB/junction. Fig. 4(c) shows the far-field image when the incident laser wavelength is changed from 1520–1570 nm. It shows that when choosing different OPA, the beam points to different direction in the same wavelength tuning range. It can be noted that OPA with large loss is easy to appear on one side of the device. We believe that one of main reason is the individual differences caused by processing errors, including optical switch and OPA.We determine the scanning angle by measuring the distance between the scanning spot and the 0 degree spot on the receiving screen. The 0 degree spot position is obtained by placing the laser pen at the chip position and emitting the laser vertically. So the measurement deviation between the two spots will bring some error on the result. After several measurements, the average value of the measurement results is taken, and error bars are specified by the maximum, minimum, and mean value of the scanning angel. As shown in Fig. 4(d), the scanning angles for the four OPAs are respectively -2.27°$\sim$5.16° ($\wedge$ = 800 nm), 5.16°$\sim$13.33° ($\wedge$ = 860 nm), 12.06°$\sim$19.98° ($\wedge$ = 920 nm) and 18.62°$\sim$26.27° ($\wedge$ = 980 nm).The tuning efficiency of the single OPA is only about 0.155°/nm on average. The steering range of the integrated four-lines chip can reach 28.54° with beam width of 2.21° and the tuning efficiency is increased to 0.57°/nm, about four times increase. However, the experimental results are 5.44° lower comparing to the simulation results which is attributed to the narrower waveguide width when the chip is manufactured. The simulation results of the waveguide grating with the width of 370 nm by FDTD are also shown in Fig. 4(d), which shows good match with our experiment. As for the horizontal direction, the far field is shown in Fig. 4(e), the position of the grating lobe is 22.78°. The intensity of the grating lobe will gradually increase with beam scanning. The beam points to 11.16° when we provided 1.0 W power to the two electrodes. In this

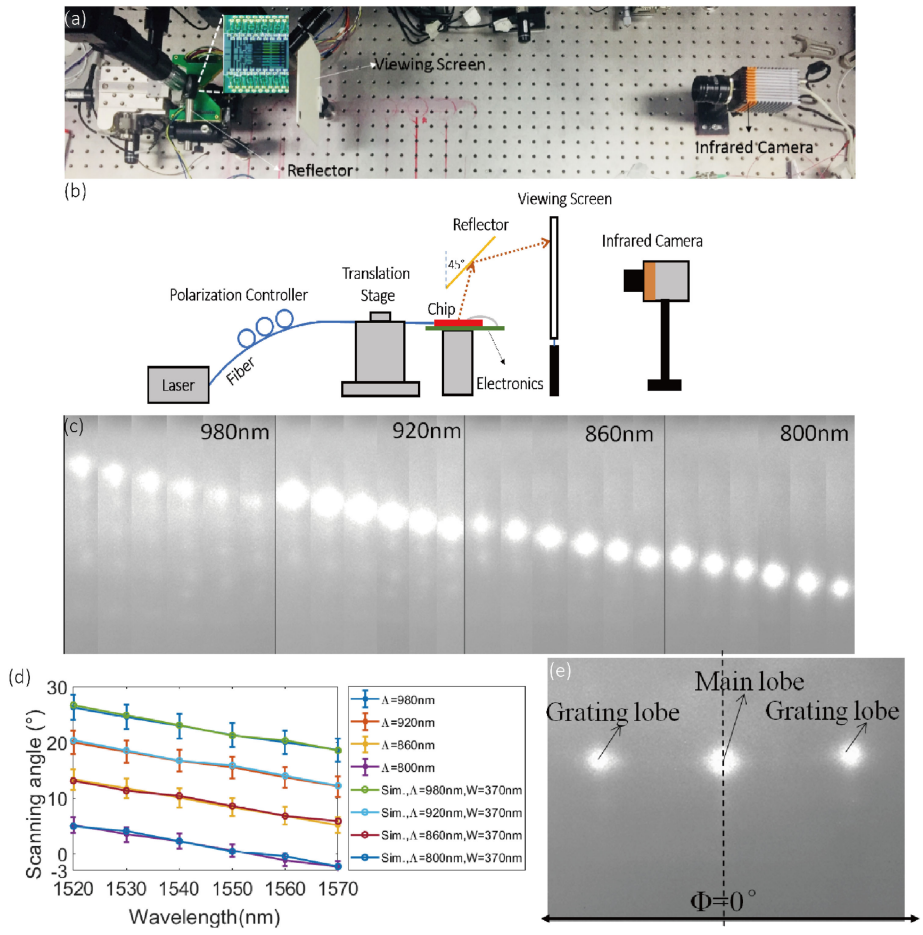

Fig. 4. (a) The characterization setup. The chip is bonded on PCB. (b) The schematic of the setup. (c) Far-field of four-lines OPA. (d) Far-field scanning angle of four-lines OPA (error bars are specified by the maximum, minimum, and mean value of the scanning angel) and the simulation results of FDTD with the waveguide width of 370 nm. The experimentation and simulation results match with each other. (e) Far-field of the one OPA in the horizontal direction.

case, the intensity of the grating lobe increases to the same as the main lobe which suggests the horizontal scanning angle of this chip is $\pm 11.16°$.

3.2 Eight-lines Optical Phased Array Beam Scanning

In order to further improve the efficiency of laser beam scattering, we propose a grating with two periods. By this way, two beams of light scan at the same time, each one scans in half area, the chip is expanded from the previous four-lines to the eight-lines chip, which is equivalent to twice the scanning efficiency. Of course, this is at the expense of reducing the laser power of each beam. In order to be able to distinguish the two beams at the receiving end, two independent detectors are needed to read them separately. The grating periods of four OPAs are 820 nm and 900 nm, 840 nm and 920 nm, 860 nm and 940 nm, 880 nm and 960 nm respectively. Adopting the optical switch to select different OPAs and control the optical wavelength from 1520 nm to 1540 nm, the far-field is shown in Fig. 5(a). It can be seen that there will be two emitted beams when a certain OPA is selected. Fig. 5(b) displays the scanning range of the chip. The scanning range of the chip are 4.58°–7.60° and 14.23°–17.77°, 7.60°–10.03° and 16.37°–19.83°, 10.22°–13.34°

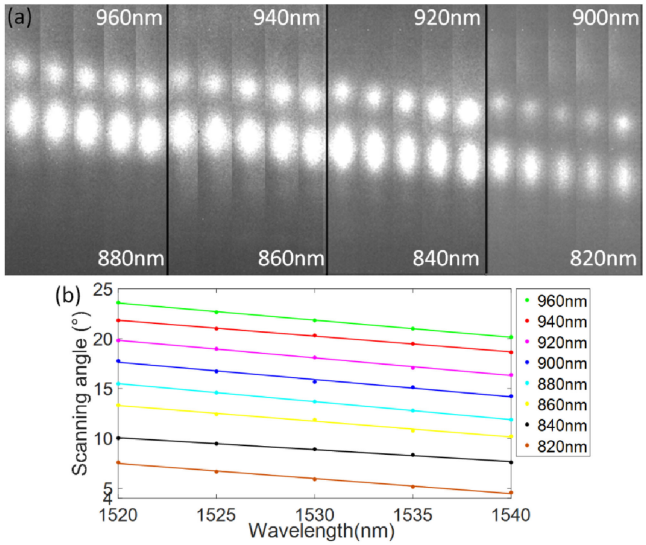

Fig. 5. (a) Far-field of eight-lines OPA. (b) Far-field scanning angles of eight-lines OPA when the wavelength tuning from 1520 nm to 1540 nm.

and 18.63°–21.83°, 11.87°–15.49° and 20.17°–23.62° when choosing the above OPA respectively. Therefore, the steering range of the eight-lines OPA covers 4.58° to 23.62° in total. It can reach 19.04° with only 20 nm wavelength limit, and the tuning efficiency is 0.95° /nm. The difference of the spot size of the two beams in each OPA is due to the different numbers of the two gratings on the waveguide, which is easy to be resolved. Compared with the above-mentioned four-lines OPA chip, the eight-lines has a higher efficiency of wavelength tuning, it can scan a larger range in a limited wavelength range. Although it has higher requirements for the detector, it has positive significance in improving the longitudinal scanning range.

4. Discussions

Table 2 summarizes the performance of longitudinal scanning of optical phased arrays using wavelength tuning. Compared with other OPA chips, the wavelength tuning efficiency of our chip is greatly improved. Tyler *et al.* integrated four OPAs (one of them cannot work due to the design error in the switching network), selecting different OPA by ring resonance switch, and realized longitudinal 3° range at 905 nm wavelength. Yet they did not conduct wavelength tuning [22]. In addition to choosing different OPAs, we also tuned the wavelength of our chip.

Because of the small grating period number, the divergence angle of our chip is large. In order to increase the grating number, generally, the waveguide is etched shallowly. For example, Intel group etched the depth only 16 nm and divergence angle reaches only 0.142° [26]. Another way is using low-index material, MIT reported several millimeters long grating using SiN [30].

5. Conclusion

We designed and demonstrated four-lines and eight-lines optical phased array chips using silicon photonics integrated circuits. The steering range of the four-lines chip reaches 28.54° in the wavelength range of 50 nm, tuning efficiency is 0.57°/nm. While the scanning range of the eight-lines chip is 19.04° with the wavelength range of 20 nm, and the tuning efficiency is 0.95°/nm. The eight-lines OPA chip can steer two beams simultaneously which greatly enhances wavelength tuning efficiency. Both these optical phased array chips have realized longitudinal large-scale

TABLE 2
Longitudinal Scanning Performance of Optical Phased Arrays

Ref.	Laser source	Numbers of waveguide	Wavelength/nm	Longitudinal scanning angle/(°)	Tuning efficiency/(°/nm)	Longitudinal beam width/(°)
[19]	off-chip	16	1525-1625	14	0.14	0.6
[20]	off-chip	16	1500-1600	15	0.15	Around 4
[21]	on-chip	32	1555-1605	3.6	0.127	0.6
[22]	off-chip	4×4	905	3	-	0.7
[23]	off-chip	16	1480-1620	20.2	0.144	2.5
[24]	off-chip	24	1540-1560	3.3	0.165	-
[25]	off-chip	16	1500-1600	14.1	0.141	2.4-2.8
[26]	on-chip	128	1260-1360	17	0.17	0.142
[27]	off-chip	512	-	14	0.3	0.15
[31]	off-chip	2×2	1545-1555	2.4	0.24	4.8(wavelength =1550 nm)
[32]	off-chip	16	1480-1580	15	0.15	0.5
[33]	off-chip	50	1454-1641	36	0.193	0.18
Four-lines in this work	off-chip	16	1520-1570	7.79	0.155	2.21
Four-lines in this work	off-chip	16×4	1520-1570	28.54	0.57	2.21
Eight-lines in this work	off-chip	16×4	1520-1540	19.04	0.95	-

scanning with a small wavelength tuning range. Next, we will integrate the semiconductor optical amplifier and the microring modulator on the chip, in order to obtain a more compact LiDAR chip.

References

[1] J. Busck and H. Heiselberg, "Gated viewing and high-accuracy three-dimensional laser radar," *Appl. Opt.*, vol. 43, no. 24, pp. 4705–4710. 2004.
[2] H. V. Duong, M. A. Lefsky, T. Ramond, and C. Weimer, "The electronically steerable flash LIDAR: A full waveform scanning system for topographic and ecosystem structure applications," *IEEE T. Geosci. Remote.*, vol. 50, no. 11, pp. 4809–4820. 2012.
[3] J. Sun, E. Timurdogan, A. Yaacobi, E. S. Hosseini, and M. R. Watts, "Large-scale nanophotonic phased array," *Nature*, vol. 493, no. 7431, pp. 195–199. 2013.
[4] P. F. Mcmanamon *et al.*, "Optical phased array technology," *Proc. IEEE*, vol. 84, no. 2, pp. 268–298. 1996.
[5] J. K. Doylend *et al.*, "Hybrid III/V silicon photonic source with integrated 1D free-space beam steering," *Opt. Lett.*, vol. 37, no. 20, pp. 4257–4259. 2012.
[6] J. Sun *et al.*, "Two-dimensional apodized silicon photonic phased arrays," *Opt. Lett.*, vol. 39, no. 2, pp. 367–370. 2014.
[7] K. Sayyah *et al.*, "Two-dimensional pseudo-random optical phased array based on tandem optical injection locking of vertical cavity surface emitting lasers," *Opt. Express*, vol. 23, no. 15, pp. 19405–19416. 2015.
[8] S. W. Chung, H. Abediasl, and H. Hashemi, "A 1024-element scalable optical phased array in 0.18 μm SOI CMOS," in *Proc. IEEE Int. Solid- State Circuits Conf. (ISSCC)*, 2017, pp. 262–264.
[9] J. Notaros, C. V. Poulton, M. J. Byrd, M. Raval, and M. R. Watts, "Integrated optical phased arrays for quasi-Bessel-beam generation," *Opt. Lett.*, vol. 42, no. 17, pp. 3510–3513. 2017.
[10] C. V. Poulton *et al.*, "Large-scale silicon nitride nanophotonic phased arrays at infrared and visible wavelengths," *Opt. Lett.*, vol. 42, no. 1, pp. 21–24. 2017.
[11] C. V. Poulton *et al.*, "Coherent solid-state LIDAR with silicon photonic optical phased arrays," *Opt. Lett.*, vol. 42, no. 20, pp. 4091–4094. 2017.
[12] T. Komljenovic and P. Pintus, "On-chip calibration and control of optical phased arrays," *Opt. Express*, vol. 26, no. 3, pp. 3199–3210. 2018.
[13] M. Zadka, Y. C. Chang, A. Mohanty, C. T. Phare, S. P. Roberts, and M. Lipson, "On-chip platform for a phased array with minimal beam divergence and wide field-of-view," *Opt. Express*, vol. 26, no. 3, pp. 2528–2534. 2018.
[14] S. H. Kim *et al.*, "Thermo-optic control of the longitudinal radiation angle in a silicon-based optical phased array," *Opt. Lett.*, vol. 44, no. 2, pp. 411–414. 2019.
[15] S. A. Miller *et al.*, "Large-scale optical phased array using a low-power multi-pass silicon photonic platform," *Optica*, vol. 7, no. 1, pp. 3–6. 2020.
[16] T. Komljenovic, R. Helkey, L. Coldren, and J. E. Bowers, "Sparse aperiodic arrays for optical beam forming and LIDAR," *Opt. Express*, vol. 25, no. 3, pp. 2511–2528. 2017.

[17] D. Zhuang *et al.*, "Omnidirectional beam steering using aperiodic optical phased array with high error margin," *Opt. Express*, vol. 26, no. 15, pp. 19154–19170. 2018.
[18] C. T. Phare, M. C. Shin, J. Sharma, S. Ahasan, H. Krishnaswamy, and A. M. Lipson, "Silicon optical phased array with grating lobe-free beam formation over 180 degree field of view," in *Proc. Conf. Lasers Electro-Optics, OSA Tech.Digest (online)(Opt. Soc. Ameri.)*, 2018, paper. SM3I.2.
[19] J. K. Doylend, M. J. R. Heck, J. T. Bovington, J. D. Peters, L. A. Coldren, and J. E. Bowers, "Two-dimensional free-space beam steering with an optical phased array on silicon-on-insulator," *Opt. Express*, vol. 19, no. 22, pp. 21595–21604. 2011.
[20] K. Van Acoleyen, W. Bogaerts, and R. Baets, "Two-dimensional dispersive off-chip beam scanner fabricated on silicon-on-insulator," *IEEE Photonics Technol. Lett.*, vol. 23, no. 17, pp. 1270–1272. 2011.
[21] J. C. Hulme *et al.*, "Fully integrated hybrid silicon two dimensional beam scanner," *Opt. Express*, vol. 23, no. 5, pp. 5861–5874. 2015.
[22] N. A. Tyler *et al.*, "SiN integrated optical phased arrays for two-dimensional beam steering at a single near-infrared wavelength," *Opt. Express*, vol. 27, no. 4, pp. 5851–5858. 2019.
[23] P. F. Wang *et al.*, "Improving the performance of optical antenna for optical phased arrays through high-contrast grating structure on SOI substrate," *Opt. Express*, vol. 27, no. 3, pp. 2703–2712. 2019.
[24] Y. Zhang *et al.*, "Sub-wavelength-pitch silicon-photonic optical phased array for large field-of-regard coherent optical beam steering," *Opt. Express*, vol. 27, no. 3, pp. 1929–1940. 2019.
[25] V. A. Karel, B. Wim, J. Jana, L. T. Nicolas, H. Romuald, and B. Roel, "Off-chip beam steering with a one-dimensional optical phased array on silicon-on-insulator," *Opt. Lett.*, vol. 34, no. 9, pp. 1477–1479. 2009.
[26] D. N. Hutchison *et al.*, "High-resolution aliasing-free optical beam steering," *Optica*, vol. 3, no. 8, pp. 887–890. 2016.
[27] S. A. Miller *et al.*, "512-element actively steered silicon phased array for low-power LIDAR," in *Proc. Conf. Lasers Electro-Opt., OSA Tech. Digest (online) (Opt. Soc. Amer.)*, 2018, paper. JTh5C.2.
[28] J. H. Kim, J. B. You, J. H. Park, K. Yu, and H. H. Park, "Design of nano-photonic phased-array antennas for wide-angle beam-steering," in *Proc. Int. Conf. Adv. Commun. Technol.*, 2016, pp. 422–425.
[29] H. Abediasl and H. Hashemi, "Monolithic optical phased-array transceiver in a standard SOI CMOS process," *Opt. Express*, vol. 23, no. 5, pp. 6509–6519. 2015.
[30] C. V. Poulton *et al.*, "Long-range LiDAR and free-space data communication with high-performance optical phased arrays," *IEEE J. Sel.Top. Quant.*, vol. 25, no. 5, pp. 1–8. 2019.
[31] V. A. Karel, R. Hendrik, and B. Roel, "Two-dimensional optical phased array antenna on silicon-on-insulator," *Opt. Express*, vol. 18, no. 13, pp. 13655–13660. 2010.
[32] D. Kwong, A. Hosseini, J. Covey, Y. Zhang, X. Xu, H. Subbaraman, and R. T. Chen, "On-chip silicon optical phased array for two-dimensional beam steering," *Opt. Lett.*, vol. 39, no. 4, pp. 941–944. 2014.
[33] C. V. Poulton, A. Yaacobi, Z. Su, M. J. Byrd, and M. R. Watts, "Optical phased array with small spot size, high steering range and grouped cascaded phase shifters," in *Proc. Adv. Photon. (IPR, NOMA, Sensors, Networks, SPPCom, SOF), OSA Tech. Digest (online) (Opt. Soc. Amer.)*, 2016, paper. IW1B.2.